Ameloblastin Amphipathic Helix Motif Mediates Ameloblast Polarization and Prismatic Enamel Formation

Gayathri Visakan[1], Rucha Arun Bapat[1], Jing Cai[1], Ethan Trevor Suwandi[2], Derk Joester[2], Natalie C Kegulian[1], Edwin Sarkisians[1], Marziyeh Aghazadeh[1], Simon Webster[1] and Janet Moradian-Oldak*[1]

1. Center for Craniofacial Molecular Biology, Herman Ostrow School of Dentistry of USC, University of Southern California, Los Angeles, CA, USA.

2. Department of Materials Science and Engineering, Northwestern University, Evanston, IL, USA

***Corresponding Author**

Janet Moradian-Oldak

joldak@usc.edu

Supplementary Information

Color Conservation Analysis

Ameloblastin protein sequences from mouse, pig and human were aligned using UniProt. The aligned FASTA sequences were analyzed for conservation using Color Conservation Analysis[1]. The threshold for identity and similarity was set at 100% and the amino acids were grouped as GAVLI, FYW, CM, ST, KRH, DENQ, P. Residues highlighted in black reveal identical residues and those in grey reveal similarity. Although the entire protein sequence was analyzed for conservation, the focus was on the AH motif contained within exon 5.

Plasmid design and protein expression and validation for recombinant mouse AmbnΔL76-P86

To generate the ΔL76–P86 deletion mutation in recombinant mouse Ambn, the previously used pET-32a plasmid expressing recombinant full-length mouse Ambn[2] was mutated using a pair of non-overlapping primers. One primer was designed to hybridize with the sense strand immediately 5’ to the 33 bases encoding the LNSLWLHGLLP amino acid sequence targeted for deletion, the other to hybridize with the antisense strand immediately 5’ to the 33 bases complementary to the bases encoding the above sequence. PCR, ligation, template removal, and transformation into NEB 5-alpha Competent *E. coli* (High Efficiency) cells were performed using the Q5 Site-Directed Mutagenesis Kit (New England Biolabs, Inc.). Plasmid was purified using the QIAprep Spin Miniprep Kit (QIAGEN), sequenced by GENEWIZ from the T7 and T7-

terminal ends to confirm successful incorporation of the ΔL76–P86 deletion, and transformed into BL21(DE3) *E. coli*, from which AmbnΔL76-P86 was expressed and purified as previously described.[3] Briefly, the *E. coli* cells were sonicated and protein affinity purified using Ni-NTA agarose columns (Qiagen). It was then dialyzed against 10kDa MWCO snakeskin dialysis membrane (Thermo) and purified using reverse phase HPLC (C4, Agilent) after removal of histidine, thioredoxin and S-tags using enterokinase (New England Biolabs) at 37℃. The protein was lyophilized overnight at -80℃ and stored at -20℃ until use. The new AH deletion mutant was characterized using 12% SDS-PAGE electrophoresis and Mass Spectrometry (ESI and MALDI). Mass spectrometry was carried out at Scripps Center for Mass Spectrometry and Metabolomics (San Diego, CA, USA). Recombinant full-length mouse Ambn and recombinant mouse AmbnΔ5 mutants were synthesized and purified as per published protocols. [2,3]

Peptide design and synthesis

Ameloblastin peptide corresponding to the multitargeting domain (MTD), xAB2, and the peptide lacking LP region residues from the MTD, xAB2ΔL76-P86 [1], were synthesized at Chempeptide Ltd. (Shanghai, China). Peptides were prepared as reported previously [4]. Peptides were reconstituted in cell culture grade PBS (Gibco) at a concentration of 10 µg/ml for cell spreading competition assays.

Transmission electron microscopy of recombinant proteins

Recombinant mouse Ambn, AmbnΔ5 and AmbnΔL76-P86, were purified and diluted to 20 µg/ml in a solution of 25 mM Tris-HCl (pH 7.4) and 150 mM NaCl. A 10 µl drop of the protein solution was applied to glow discharged carbon grids (01814-F Support Film, Carbon Type-B 400 mesh, Copper, Ted Pella) and incubated for 5 minutes at room temperature. The grid was blotted using filter paper and immediately negatively stained with 2% uranyl acetate in deionized water for 10 seconds (5 seconds for AmbnΔL76-P86), then blotted again and air dried. The grids were examined using transmission electron microscopy (Talos F200C G1 Biological TEM, FEI, OR, USA) with an accelerating voltage of 80 kV.

Dynamic Light Scattering analysis of recombinant proteins

Full-length recombinant mouse Ambn and recombinant AmbnΔL76-P86 were diluted individually to 3 µM in 50 mM Tris, 50 mM NaCl buffer at pH 7.6. Diluted samples were allowed to stand at room temperature for 1 h. Immediately prior to measurement, recombinant mouse Ambn was centrifuged for 5 min at 12,000 rpm to get rid of larger aggregates. No large aggregates were observed in recombinant mouse AmbnΔL76-P86 and hence the mutant protein was not centrifuged. Samples were placed in a 10 µl quartz cuvette and measured at room temperature

using a DynaPro NanoStar light scattering instrument (Wyatt). Ten acquisitions were performed with each being an average of ten scans for one experiment. Each experiment was repeated at least three times, with a fresh dilution of protein prepared each time. Particle size distribution is reported as hydrodynamic radii based on a Rayleigh sphere model. For each curve showing particle size distribution, an intensity autocorrelation curve was simultaneously measured. Data were analyzed using Dynamics 7.1.1 and plotted in Microsoft Excel.

Optical microscopy

Both whole heads and hemi-mandibles from 7-week-old *Ambn*$^{WT/WT}$, *Ambn*$^{\Delta L76\text{-}P86\ +/-}$ and *Ambn*$^{\Delta L76\text{-}P86\ -/-}$ mice were examined under a dissecting microscope (Olympus, CKX53). Images were recorded for the examination of gross-enamel appearance of incisors (whole heads).

Enamel mineral density and thickness measurements from conventional micro-CT

Qualitative analysis of incisor enamel mineral density was carried out in three-dimensional sagittal reconstructions of mandibles from seven-week-old (7W) *Ambn*$^{WT/WT}$, *Ambn*$^{\Delta L76\text{-}P86\ +/-}$ and *Ambn*$^{\Delta L76\text{-}P86\ -/-}$ mice. Using heatmap renderings, incisor enamel mineral density along the sagittal plane was examined in the *Ambn*$^{\Delta L76\text{-}P86}$ mutants and compared to *Ambn*$^{WT/WT}$. Commercial hydroxyapatite phantoms corresponding to mineral densities of 0.25 g/cm^3 and 0.75 g/cm^3 were used to calibrate the micro-CT system. An equation correlating mineral density and attenuation co-efficient was derived from the phantom scans and was used to measure mineral density of incisor enamel using the CTAn (software version 1.6.9.8; SkyScan). Four regions were identified on sagittal sections of incisors based on anatomical landmarks for measurement of enamel mineral density (Supplementary Figure 2). Relative enamel mineral density values corresponding to regions A - D were obtained by normalizing against region D of *Ambn*$^{WT/WT}$ (corresponding to erupted enamel) and were plotted for the *Ambn*$^{\Delta L76\text{-}P86}$ mutants and *Ambn*$^{WT/WT}$ and absolute enamel mineral density values from region D (corresponding to erupted enamel) were analyzed and compared for statistical significance. 7W samples were used to measure and compare the enamel thickness. Five different samples were measured for enamel thickness at region C (which corresponds to the unerupted enamel). Heatmap rendering of axial incisor sections was used for measuring enamel thickness. Results were tabulated and analyzed for statistical significance using GraphPad Prism version 10.4.1.

High resolution micro-CT, Segmentation, and Analysis of Reconstructions

High resolution micro-CT was performed at the Molecular Imaging Center at the Department of Radiology (University of Southern California, CA, USA). Hemimandibles for analysis using a SCANCO µCT50 instrument were mounted on a custom-designed, 3D-printed holder such that

the long axis of the incisor was aligned with the rotation axis. An aluminum wire (>99.99%, *d* = 500 µm, Sigma Aldrich) of length equal to or exceeding that of the hemimandible was mounted adjacent to the incisor as an attenuation standard. The µCT50 was operated at 70 kVp and 85 µA. Three-dimensional reconstructions with an isotropic voxel pitch of 6 µm ("high resolution") were generated using NRecon (version 1.6.9.8).

High-resolution reconstructions were segmented into seven classes (background, bone, incisor enamel, incisor dentin, molar enamel, molar dentin, and Al wire) using a convolutional neural network (CNN) trained as previously described [5,6] but re-implemented in Python.[7] Segmentations were manually cleaned up using Dragonfly version 2022.2 (Object Research Systems Inc). Downstream processing was implemented in Python, drawing specifically on the SciPy, NumPy, pandas, Matplotlib, xarray, and PyVista libraries. [8-13]

Linear attenuation coefficients (μ, LAC) were calculated for each slice normal to the z-direction (the axis of rotation) separately, using

$$\mu_k(i,j) = \frac{I_k(i,j) - \bar{I}_k^{\mathrm{bkg}}}{\bar{I}_k^{\mathrm{Al}} - \bar{I}_k^{\mathrm{bkg}}} \left(\mu_{Al} - \mu_{\mathrm{bkg}}\right) + \mu_{\mathrm{bkg}}$$

where $I_k(i,j)$ is the intensity of the voxel with indices *i* in the *x*-direction and *j* in the *y*-direction in the k^{th} slice in the *z*-direction, $\bar{I}_k^{\mathrm{bkg}}$ is the mean intensity of all voxels in the background class within the k^{th} slice, $\bar{I}_k^{\mathrm{Al}}$ the mean intensity of all voxels in the Al wire class within the k^{th} slice, μ_{Al} the calculated LAC of aluminum, and $\mu_{\mathrm{bkg}} = 0$ the estimated LAC of the background. The value for μ_{Al} for the polychromatic source with a maximum photon energy of 70 kVp was estimated as

$$\mu_{\mathrm{Al}} = \left(\frac{\mu}{\rho}\right)_{\mathrm{Al}} \rho_{\mathrm{Al}}$$

, where $(\mu/\rho)_{Al} = 0.848\ \mathrm{cm}^2 \cdot \mathrm{g}^{-1}$ is the mass attenuation coefficient for aluminum at a photon energy of 35 keV (the approximate average photon energy given the maximum of 70 kVp) and $\rho_{\mathrm{Al}} = 2.699\ \mathrm{g} \cdot \mathrm{cm}^{-3}$. [14]

For visualization of the enamel mineral density, only voxels that were at least 15 µm below the enamel surface were included. The volumetric density maps were smoothed using a Gaussian filter (standard deviation 6 µm, kernel size 9x9x9 voxels).

Incisor enamel thickness and tissue mineral density were determined as a function of arc length *L* along the incisor. For this purpose, an osculating circle with radius $\hat{R}$ was fitted to the dentino-enamel junction (DEJ) as will be described in a separate publication. The center of the circle

and its normal vector were used to define a cylindrical coordinate system (r, θ, z). The arc length $L = \theta \hat{R}$ increases in the cervical-to-incisal direction and was referenced to the azimuthal angle of the centroid of the distal root canal of the M_1 molar. Voxels in the incisor enamel class were sorted into bins with width $\Delta\theta = \Delta L/\hat{R}$, where ΔL = 10 μm.

For each voxel in the incisor enamel class, the distance to the closest voxel in the incisor dentin class was calculated using a distance transform. The maximum enamel thickness was then calculated as the upper extreme (maximum) of the distance distribution for each bin.

To determine the mean tissue mineral density ρ_{TMD}, the linear attenuation coefficient for voxels in the incisor enamel class μ were converted using

$$\rho_{\mathrm{TMD}} = \mu \left(\frac{\mu}{\rho}\right)^{-1}_{\mathrm{OHAp}}$$

, where $(\mu/\rho)_{OHAp} = 1.543\ \mathrm{cm}^2 \cdot \mathrm{g}^{-1}$ is the mass attenuation coefficient for stochiometric hydroxylapatite and then averaged for each bin.

For both maximum thickness and tissue mineral density, group averages were calculated per bin and then smoothed using a moving average filter with a window that extended 50 μm on either side. The associated 95% confidence interval for arc length L was calculated as

$$CI(L) = \pm 1.96 \frac{\bar{\sigma}(L)}{\sqrt{n(L)}}$$

where $\bar{\sigma}(L)$ is the moving standard deviation and $n(L)$ the moving sample count, determined over the same window. The moving sample count is the number of samples in the group that contributed data in the window (equal to the total number of samples in the group where incisors overlap in arc length).

qPCR

Post-natal 5 days old (P5) 1st molars, which are representative of secretory stage of amelogenesis were used. Enamel organs (from 5 animals in each group) were dissected and RNA was extracted using an RNeasy Plus Mini Kit (Qiagen) according to the manufacturer's instructions. The extracted RNA was reverse transcribed using iScript Reverse Transcription Supermix for RT-qPCR (Bio-rad). The reverse-transcribed cDNA from *Ambn*$^{WT/WT}$ and *Ambn*$^{\Delta L76\text{-}P86}$ mutants was used to determine the relative expression levels of *AmelX* and *Ambn* using the CFX96 Real-Time System (Bio-rad) with iQ SYBR Green Supermix (Bio-rad). The primer

sequences are outlined in Supplementary Table 1. Results were analyzed for statistical significance using GraphPad Prism version 10.4.1.

Bulk RNA sequencing

Ten mandibular 1st molar enamel organs from five P5 pups of each genotype were pooled for RNA isolation. Pups in each group were from at least two different litters. RNA was isolated from the pooled tissue using an RNeasy Plus mini kit (Qiagen 74134) according to the manufacturer's instructions. A preliminary RNA quality check was performed using a NanoDrop™. One Microvolume UV-Vis Spectrophotometer (Thermo Scientific, Catalog number ND-ONE-W). RNA samples with an A260/280 ratio of approximately 2.0 and an A260/230 ratio between 2.0-2.2 were used for further analysis. A second quality check was performed by Novogene, using an Agilent Bioanalyzer. Only samples with RNA integrity number (RIN) > 7 were used for sequencing (n=3 for $Ambn^{\Delta L76\text{-}P86\ +/-}$ and $Ambn^{WT/WT}$, n=4 for $Ambn^{\Delta L76\text{-}P86\ -/-}$). RNA sequencing, including mRNA library preparation (polyA enrichment), was performed by Novogene. The data were acquired using NovaSeq X Plus Series (PE150) sequencer at a sequencing depth of 20 million paired end reads. Data were analyzed using Partek Flow. Three or four samples per genotype of trimmed paired-end reads were aligned to mouse genome GRCm39 (Gencode release M33) using STAR alignment and default parameters. Quantification was performed using Partek E/M algorithm with M33 annotation and strict paired-end compatibility. Genes with maximum counts <= 10 across all samples were filtered and normalization was performed using upper quartile normalization and 'add 1'. Pairwise DESeq2 analysis was used to determine differentially expressed genes, and the results were filtered for fold change ±1.5 and p value ≤ 0.05. Gene Ontology (gene set enrichment) and KEGG pathway analyses were performed in Partek flow, using the filtered gene list. Since enamel matrix proteins or proteases of interest (Amelogenin, Ameloblastin, Enamelin, Odam, MMP20 and KLK4) did not appear as differentially expressed, raw normalized gene counts of each of the above genes were plotted to show their expression levels in mutants and WT. The plot was created in GraphPad Prism version 10.5.0.

Immunofluorescent labeling of P8 incisors

P8 mandibular incisors were used for all the immunolabeling experiments. Paraffin sections of 7 µm thickness along the sagittal orientation were prepared, to visualize incisor ameloblasts. For labeling of full-length Ambn, antigen retrieval was carried out overnight in citrate buffer (1mM sodium citrate dihydrate, pH 6.0) at 70℃. For all other immunolabeling experiments, slides were dehydrated for 1h at 60℃ in a hot air oven followed by rehydration in xylene (100%) and ethanol gradient (100%, 95%). Antigen retrieval was then performed by boiling either in Tris-EDTA buffer

(10 mM Tris Base, 1 mM EDTA, 0.05% Tween 20, pH 9.0) or citrate buffer (depending on antibody manufacturer's recommendations) for 22 mins at 100℃ followed by cooling for 22 mins at room temperature. Endogenous peroxidases and enamel autofluorescence were blocked using 0.3% H_2O_2 treatment for 30 mins. Slides were blocked using 3% bovine serum albumin (BSA), 10% donkey serum, and 0.05% Tween 20 for 2 h at room temperature. Slides were then incubated with primary antibody (diluted with 10% donkey serum and 0.05% Tween 20) overnight at room temperature in a moist chamber. Slides were incubated with secondary antibodies at room temperature in a moist chamber for 2 h. Nuclei were counterstained with 1:1000 DAPI. Samples were then mounted with Vectashield (Vector Laboratories) and coverslips were sealed with nail varnish and stored at 4℃ prior to imaging.

TUNEL Labeling

Cell apoptosis in *Ambn*$^{WT/WT}$ and *Ambn*$^{\Delta L76\text{-}P86}$ mutants was examined using the TUNEL method, using Terminal Deoxynucleotidyl Transferase (TdT) to catalyze the incorporation of CoraLite 488-conjugated dUTP (CL488-dUTP) at the 3'-OH end of the broken DNA in apoptotic cells. P8 incisors were used to carry out TUNEL labeling using standard protocols recommended by the manufacturer (PF00006 Proteintech). Slides were rehydrated in ascending ethanol rinses after immersion in xylene. Slides were treated with 20 µg/ml proteinase K in 1X PBS for 15 mins at room temperature. Terminal dUTP nick end labeling was carried out by incubating slides with CL488-dUTP in TUNEL reaction buffer containing TdT enzyme for 2h in the dark. Positive controls were pre-treated with DNase I (20 U/mL) and negative controls were incubated with TUNEL reaction mixture without TdT. Slides were rinsed with 5 mg/mL BSA with 0.1% Triton X-100 in PBS to remove background labeling. Nuclei were counterstained with DAPI. Samples were mounted and coverslips sealed with nail varnish. Cells were visualized using confocal microscopy (Stellaris, Leica) and tile-scans were recorded to examine TUNEL and DAPI co-labeling. The experiment was repeated thrice.

Direct cell spreading assay using recombinant proteins and ameloblast lineage cells (ALC)

An established protocol for cell spreading competition assays was used with some modifications. [15] Briefly, 96-well plates (Cellstar) were coated by incubation with 100 µl of 10 µg/ml recombinant protein diluted in cell culture-grade PBS (Gibco) overnight at 4℃. The following proteins were used: recombinant mouse Ambn or recombinant AmbnΔL76-P86. In the non-coated controls, wells were incubated with PBS alone. The wells were blocked with 200 µl of 10 mg/ml heat-denatured BSA for 1h at room temperature. ALC were trypsinized and resuspended in DMEM (without FBS) buffered with 20 mM HEPES at a density of 1.0 x 10^4

cells/well. Cells were then overlaid with an equal volume of 1X PBS and incubated at 37℃ for 90 mins. Cells were fixed with 5% v/v glutaraldehyde, stained with 0.1% crystal violet and visualized using a Keyence BZX710 microscope. The ratio of the number of cells that adopted a spread morphology to the total number of cells was determined using ImageJ. The experiment was carried out in duplicate and repeated thrice.

ALC spreading competition assay using synthetic Ambn peptides

Established protocols for cell spreading competition assays were used.[15,16] 96-well plates (Cellstar) were coated with 100 µl of 10 µg/ml recombinant mouse Ambn in cell culture-grade PBS overnight at 4℃. The plates were blocked with 200 µl of 10 mg/ml heat-denatured BSA for 1h at room temperature. ALC were trypsinized and resuspended in DMEM buffered with 20 mM HEPES and allowed to incubate at 37℃ for 15 min at a resuspension density of 0.5 x 10^4 cells/well. The cells were treated with 10 µg/ml of xAB2, xAB2∆L76-P86 peptide, or PBS. This mixture of cells and peptides was added to the wells, and the plates were incubated at 37℃ for 90 min. The cells were fixed with 5% v/v glutaraldehyde, stained with 0.1% crystal violet, and visualized with a Keyence BZX710 microscope. The ratio of the number of cells that adopted a spread morphology to the total number of cells was determined using ImageJ. The experiment was carried out in duplicate and repeated thrice.

3D cell culture and aspect ratio measurements (ALC)

Pre-chilled glass-bottomed 96-well plates (Mattek) were coated with 20 μg/ml test (recombinant mouse Ambn∆L76-P86) and control (heat-denatured recombinant mouse Ambn, and WT recombinant Ambn) proteins. Ice-cold, growth-factor-reduced Geltrex (Thermo) was overlaid on coated plates and incubated at 37℃ for 30 min. ALC were detached from culture dishes at 80% or greater confluence and were centrifuged at 200 x g for 5 mins to obtain a soft pellet. The cells were resuspended in DMEM (with FBS) and inoculated atop set GFR Geltrex gels at a cell seeding density of 3.5 x 10^4 cells/well. Cells were allowed to attach to the gel for 30 mins at 37℃. Following cell attachment, a 10% v/v gel coat in cell culture media was overlaid on the cells to create a 3D-on-top-type culture. These 3D gels were incubated at 37℃ in a standard cell culture incubator for 24 h. Cells were fixed with 25% glutaraldehyde for 15 min at room temperature. Cells in the 3D gel were labeled with 1:1000 DiD and 1:1000 DAPI and were visualized using a Keyence BZX810 microscope with a PlanApo λ objective (NA = 0.75). Sequential Z-stacks were recorded with a pitch of 0.4 µm. Z-stacks were reconstructed using the Keyence Image Viewer (software version 1.1.1.8), and the 3D measure-tool was used to record the cell width along the XY plane and cell height along the Z axis. These values were tabulated, and the aspect ratio was calculated. Repeated measurements of aspect ratio were

recorded to analyze for statistical significance using GraphPad Prism version 10.4.1. and the experiments were repeated three times.

Supplementary Table 1

AmelX	F- GTCACCTCTGCATCCCATG
	R- TTCCCGCTTGGTCTTGTC
Ambn	F- CTGTTACCAAAGGCCCTGAA
	R- GCCATTTGTGAAAGGAGAG

Supplementary Table 1. Primer sequences for qPCR for amelogenin *(AmelX)* and ameloblastin *(Ambn)*

Supplementary Table 2

Gene ID	Gene name	p-value	Fold change
ENSMUSG00000044864.17	Ankrd50	2.4511e-2	-1.6036
ENSMUSG00000014498.10	Ankrd52	3.2699e-2	-1.7282
ENSMUSG00000032375.16	Aph1b	1.3529e-2	-1.6717
ENSMUSG00000029787.11	Avl9	1.8991e-2	-1.9402
ENSMUSG00000037458.16	Azin1	1.8509e-2	-1.5492
ENSMUSG00000066324.3	Bpnt2	1.2999e-4	-1.7501
ENSMUSG00000025103.9	Btbd1	8.3792e-3	-1.5849
ENSMUSG00000062098.12	Btbd3	1.7204e-3	-1.9455
ENSMUSG00000037493.7	Cib2	2.2216e-2	1.9604
ENSMUSG00000046798.15	Cldn12	1.7475e-2	-1.7672
ENSMUSG00000022037.16	Clu	2.2769e-2	1.6781
ENSMUSG00000028626.6	Col9a2	4.5060e-2	1.6835
ENSMUSG00000046516.12	Cox17	3.5033e-2	1.6690
ENSMUSG00000022742.7	Cpox	1.7066e-2	-1.8224
ENSMUSG00000001622.16	Csn3	4.5891e-2	-1.6627
ENSMUSG00000051674.16	Dcun1d4	2.8100e-2	-1.7596
ENSMUSG00000117748.2	Derpc	3.2616e-3	3.0178
ENSMUSG00000014905.5	Dnajb9	1.2206e-2	-1.5991
ENSMUSG00000058325.7	Dock1	3.9304e-2	-1.6614
ENSMUSG00000096255.3	Dynlt1b	2.6358e-2	1.8597
ENSMUSG00000038418.8	Egr1	5.9382e-3	2.2986

ENSMUSG00000020715.10	Ern1	1.7012e-2	-1.8838
ENSMUSG00000027654.3	Fam83d	2.1522e-2	1.9098
ENSMUSG00000020635.9	Fkbp1b	7.5995e-3	1.9237
ENSMUSG00000033487.15	Fndc3a	2.0798e-2	-1.8037
ENSMUSG00000000420.16	Galnt1	1.0302e-2	-1.6055
ENSMUSG00000086845.2	Gm13010	3.9792e-3	2.3398
ENSMUSG00000031517.9	Gpm6a	1.4070e-2	-1.6179
ENSMUSG00000047875.7	Gpr157	2.2876e-2	-1.5451
ENSMUSG00000056999.17	Ide	1.7475e-2	-1.5848
ENSMUSG00000053560.6	Ier2	4.1815e-2	1.5445
ENSMUSG00000029814.11	Igf2bp3	4.7702e-2	-1.6062
ENSMUSG00000027598.17	Itch	4.4333e-2	-1.5421
ENSMUSG00000030102.12	Itpr1	1.1263e-2	-1.9123
ENSMUSG00000045312.13	Lhfpl2	3.2480e-2	-1.6344
ENSMUSG00000026623.17	Lpgat1	2.3443e-2	-1.6011
ENSMUSG00000070639.6	Lrrc8b	1.2128e-2	-1.6047
ENSMUSG00000074622.5	Mafb	1.1413e-2	-1.5014
ENSMUSG00000003746.17	Man1a	3.1410e-2	-1.5128
ENSMUSG00000020623.12	Map2k6	2.6838e-2	-1.7348
ENSMUSG00000027239.15	Mdk	4.2353e-2	1.6897
ENSMUSG00000038022.12	Mindy4	4.0224e-2	1.8198
ENSMUSG00000064363.1	mt-Nd4	4.1277e-2	1.6349
ENSMUSG00000064367.1	mt-Nd5	4.2622e-2	1.6316
ENSMUSG00000022194.16	Pabpn1	4.0369e-2	1.5487
ENSMUSG00000022438.7	Parvb	8.7683e-3	-1.5049
ENSMUSG00000024122.17	Pdpk1	4.9728e-2	-1.7365
ENSMUSG00000041731.14	Pgm5	2.9254e-2	-1.5078
ENSMUSG00000024867.15	Pip5k1b	1.8209e-2	-1.5957
ENSMUSG00000024083.17	Pja2	4.0910e-2	-1.5984
ENSMUSG00000030701.18	Plekhb1	3.2652e-2	-1.7886
ENSMUSG00000033152.14	Podxl2	3.1393e-2	1.5856
ENSMUSG00000038582.16	Pptc7	3.5925e-2	-1.7621
ENSMUSG00000025742.6	Prps2	1.0345e-2	-1.5302
ENSMUSG00000037992.17	Rara	4.7623e-2	1.5210
ENSMUSG00000002233.14	Rhoc	3.2772e-2	1.6562

ENSMUSG00000047496.7	Rnf152	2.3191e-2	-1.7876
ENSMUSG00000027907.5	S100a11	4.9457e-2	1.5285
ENSMUSG00000001025.9	S100a6	4.3600e-2	1.6940
ENSMUSG00000028082.15	Sh3d19	2.0034e-2	-1.6505
ENSMUSG00000031596.16	Slc7a2	1.7285e-3	-2.0075
ENSMUSG00000090084.8	Srpx	1.1154e-2	1.6888
ENSMUSG00000047904.7	Sstr2	3.9460e-2	-1.5915
ENSMUSG00000040287.10	Stac3	4.5713e-2	1.8773
ENSMUSG00000028643.12	Svbp	4.4628e-2	1.7327
ENSMUSG00000052415.6	Tchh	1.3176e-3	-2.7134
ENSMUSG00000040152.9	Thbs1	6.4923e-3	1.6736
ENSMUSG00000030516.15	Tjp1	2.5457e-2	-1.6413
ENSMUSG00000024642.18	Tle4	4.2947e-2	-1.5039
ENSMUSG00000061451.14	Tmem151a	1.2320e-2	1.5615
ENSMUSG00000058587.10	Tmod3	2.7502e-2	-1.5038
ENSMUSG00000030306.15	Tmtc1	1.5816e-2	-1.7420
ENSMUSG00000062210.14	Tnfaip8	1.2268e-2	-1.5182
ENSMUSG00000012535.15	Tnpo3	3.7567e-2	-1.5471
ENSMUSG00000028464.17	Tpm2	1.9344e-2	1.6956
ENSMUSG00000071660.11	Ttc9c	3.6367e-2	-1.7850
ENSMUSG00000032020.16	Ubash3b	2.8714e-2	-1.6636
ENSMUSG00000044308.18	Ubr3	4.9413e-2	-1.5549
ENSMUSG00000026728.10	Vim	2.0354e-2	1.5726
ENSMUSG00000020218.12	Wif1	8.9051e-3	1.5605

Supplementary Table 2. Differentially expressed genes from *Ambn*$^{WT/WT}$v *Ambn*$^{\Delta L76\text{-}P86\ -/-}$

Supplementary Table 3

Gene ID	Gene name	p-value	Fold change
ENSMUSG00000032375.16	Aph1b	4.1315e-2	-1.5274
ENSMUSG00000032373.16	Car12	2.7874e-2	-2.0874
ENSMUSG00000073802.6	Cdkn2b	4.0283e-4	-2.6839
ENSMUSG00000001622.16	Csn3	4.7447e-3	-2.0528
ENSMUSG00000117748.2	Derpc	2.4945e-3	3.1108
ENSMUSG00000030986.14	Dhx32	1.6581e-2	-1.5488

ENSMUSG00000027224.15	Duoxa1	1.5509e-2	-1.9184
ENSMUSG00000041773.9	Enc1	4.3254e-2	-1.6299
ENSMUSG00000071984.13	Fndc1	4.2774e-2	-2.0576
ENSMUSG00000066571.14	Garre1	3.4544e-2	-2.0679
ENSMUSG00000003316.15	Glg1	2.6161e-2	-1.5478
ENSMUSG00000082536.2	Gm13456	1.2226e-2	-1.6981
ENSMUSG00000006948.8	Klk4	1.9679e-3	-2.4341
ENSMUSG00000058354.8	Krt6a	3.4457e-2	-3.4732
ENSMUSG00000042793.14	Lgr6	8.3322e-3	-1.7375
ENSMUSG00000045312.13	Lhfpl2	4.4497e-2	-1.5863
ENSMUSG00000022438.7	Parvb	8.2395e-3	-1.5095
ENSMUSG00000102918.2	Pcdhgc3	7.8574e-3	-1.8629
ENSMUSG00000022951.19	Rcan1	7.2036e-5	-2.8550
ENSMUSG00000002633.5	Shh	2.2528e-2	1.6481
ENSMUSG00000041771.15	Slc24a4	2.9332e-4	-3.4941
ENSMUSG00000046959.17	Slc26a1	1.1124e-3	-2.6782
ENSMUSG00000027737.11	Slc7a11	1.9762e-2	-1.8954
ENSMUSG00000090084.8	Srpx	1.9893e-2	1.6172
ENSMUSG00000042066.17	Tmcc2	2.4658e-2	-1.8022
ENSMUSG00000054871.6	Tmem158	1.4369e-2	-1.9360
ENSMUSG00000028464.17	Tpm2	2.4643e-2	1.6603
ENSMUSG00000030471.18	Zdhhc13	2.9521e-2	-1.8359

Supplementary Table 3. Differentially expressed genes from *Ambn*$^{WT/WT}$ v *Ambn*$^{\Delta L76\text{-}P86\ +/-}$

Supplementary Figure 1

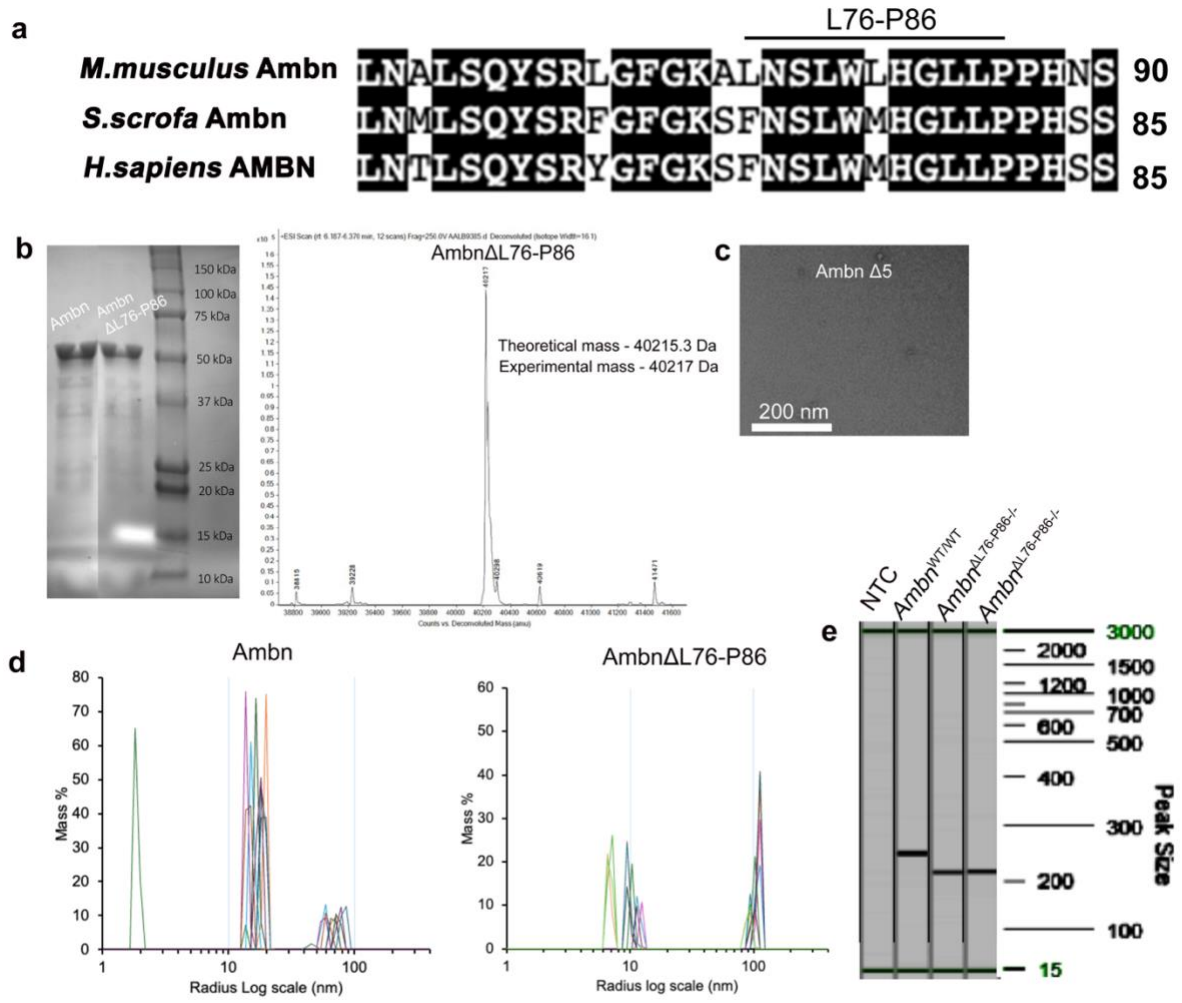

Supplementary Figure 1. Rationale for design of Ambn$^{\Delta L76\text{-}P86}$ mutants. (**a**) Color Conservation Analysis of ameloblastin amphipathic helix motif region from representative mammals. Residues highlighted in black show 100% sequence identity. The LP region spanning Lys76 to Pro86 is highlighted on the top. (**b**) Characterization of recombinant mouse LP deletion mutant protein using 12% SDS PAGE electrophoresis (left) and Mass Spectrometry ESI analysis (right). (**c**) Transmission electron microscopy analysis of recombinant mouse Ambn∆5 protein lacking the sequence encoded by exon 5, showing lack of self-assembly. (**d**) Dynamic Light Scattering (DLS) of recombinant mouse Ambn (left) and recombinant mouse AmbnΔL76-P86 (right). (**e**) Agarose gel electrophoresis of *Ambn*$^{\Delta L76\text{-}P86}$ mutants. One male and female sample are shown. Genotyping analysis performed at UC Davis.

Supplementary Figure 2

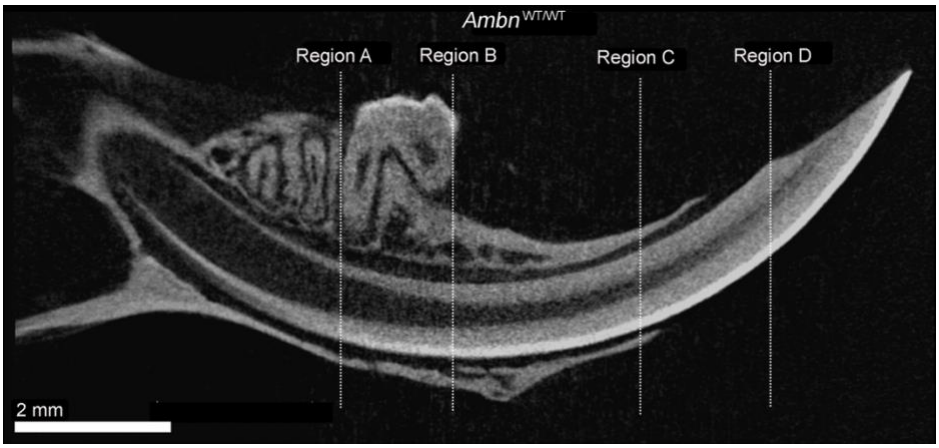

Supplementary Figure 2. Sagittal slice through micro-CT reconstruction of seven-week-old mandible from *Ambn*$^{WT/WT}$ showing anatomical landmarks used for enamel mineral density measurements.

Supplementary Figure 3

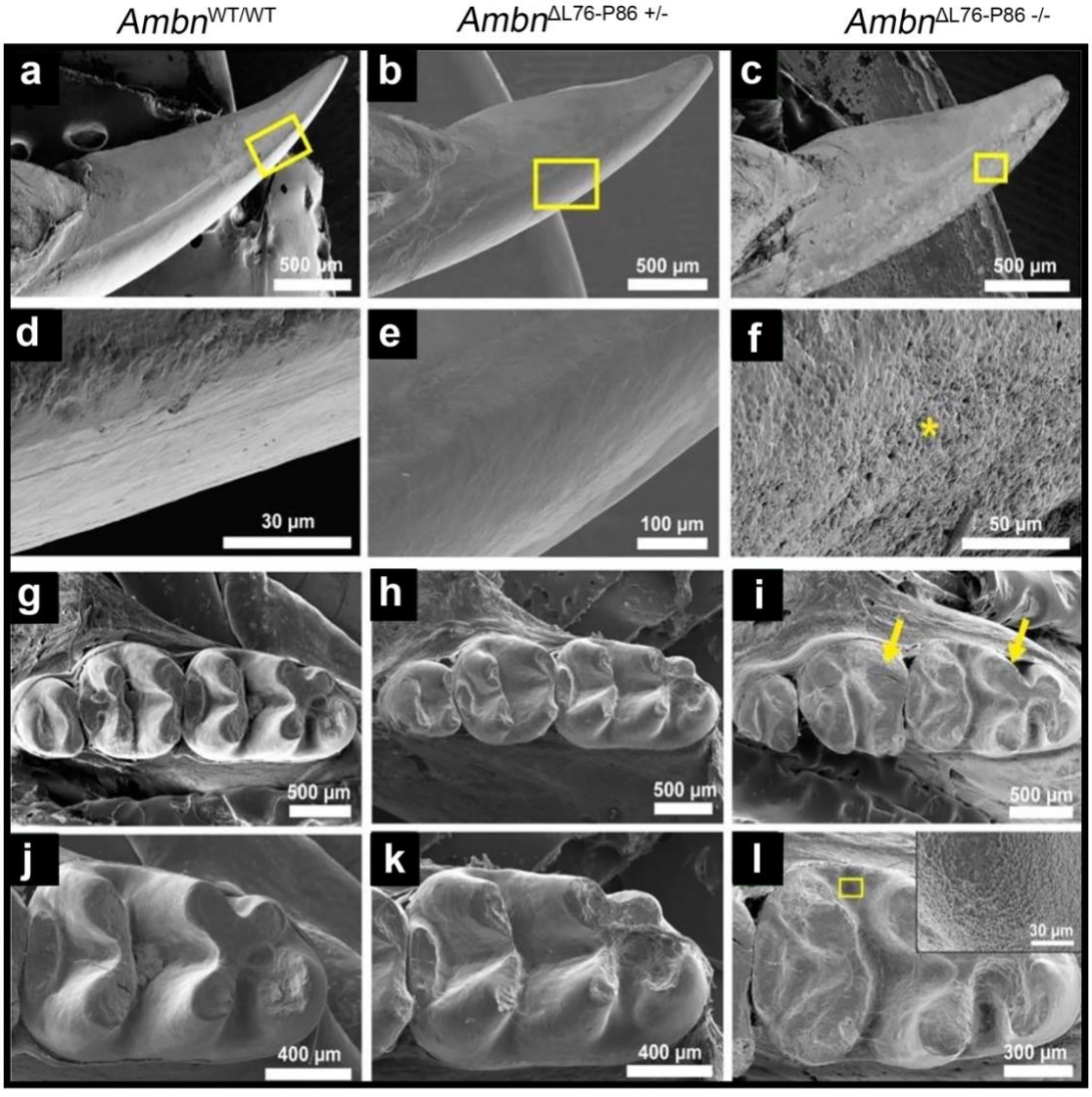

Supplementary Figure 3. Scanning electron microscopy analysis of 7-week-old incisors (top two panels) and molars (bottom two panels) from *Ambn*$^{WT/WT}$ and *Ambn*$^{\Delta L76\text{-}P86}$ mutants. (**a - c**) Low resolution images from the labial surface of incisors from *Ambn*$^{WT/WT}$ (a), *Ambn*$^{\Delta L76\text{-}P86\ +/-}$ (b), and *Ambn*$^{\Delta L76\text{-}P86\ -/-}$(c). Yellow squares indicate the locations from where high-resolution images were recorded. (**d - f**) High resolution images from the labial surface of incisors from *Ambn*$^{WT/WT}$ (d), *Ambn*$^{\Delta L76\text{-}P86\ +/-}$ (e), and *Ambn*$^{\Delta L76\text{-}P86\ -/-}$ (f). (**g - i**) Low resolution images from the occlusal surface of molars from *Ambn*$^{WT/WT}$ (g), *Ambn*$^{\Delta L76\text{-}P86\ +/-}$ (h), and *Ambn*$^{\Delta L76\text{-}P86\ -/-}$(i). Yellow arrows in I indicate significant wear of occlusal tips of molars resulting in a flat occlusal plane in *Ambn*$^{\Delta L76\text{-}P86\ -/-}$ mutants. (**j - l**) High resolution images from the occlusal surface of molars from *Ambn*$^{WT/WT}$ (j), *Ambn*$^{\Delta L76\text{-}P86\ +/-}$ (k), and *Ambn*$^{\Delta L76\text{-}P86\text{-}/-}$ (l). Inset in L shows increased surface roughness on the slopes of the molar cusps in *Ambn*$^{\Delta L76\text{-}P86\ -/-}$.

Supplementary Figure 4

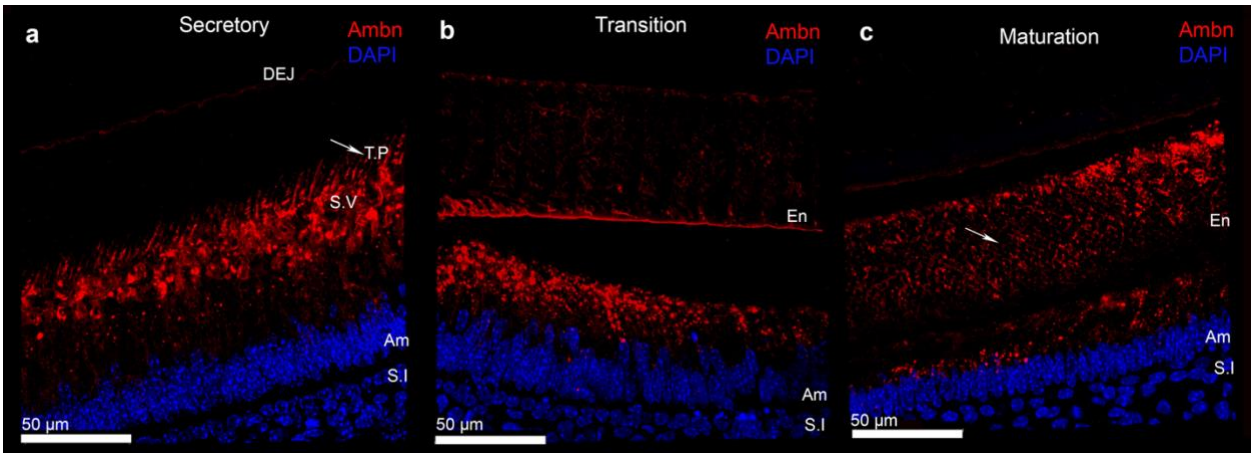

Supplementary Figure 4. (a - c) Custom N-terminal Ambn peptide antibody characterization using stagewise immunolabeling of post-natal 8-day old incisors from *Ambn*$^{WT/WT}$ in secretory stage (a), transition stage (b) and maturation stage (c) of amelogenesis. White arrow indicates labeling along the Tomes' processes in secretory stage in (a) and the immunolabeling pattern in the extracellular matrix in maturation stage in (c). En- enamel, T.P- Tomes' Processes, S.V- secretory vesicles, Am- ameloblast, S.I stratum intermedium.

Supplementary Figure 5

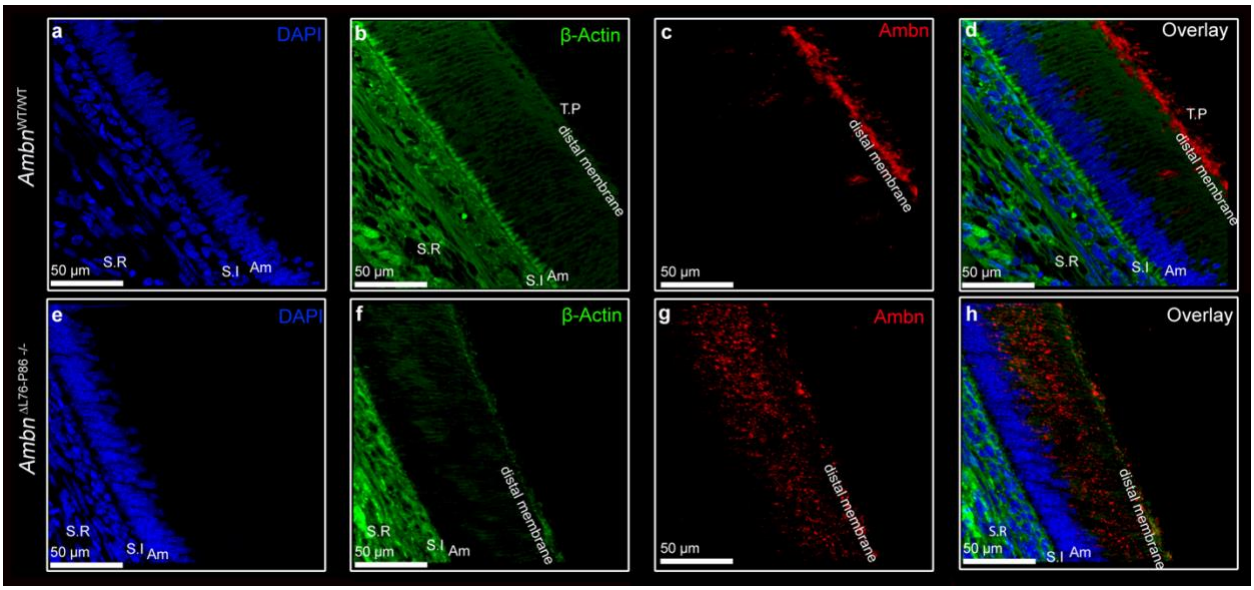

Supplementary Figure 5. Custom N-terminal anti-Ambn antibody co-labeling with anti-β-actin antibody in secretory stage. (**a - d**) Secretory stage incisors from *Ambn*$^{WT/WT}$ co-labeled with N-terminal anti-Ambn antibody and anti-β-actin. (**e - h**) Secretory stage incisors from *Ambn*$^{\Delta L76\text{-}P86\ -/-}$ mutant co-labeled with N-terminal anti-Ambn antibody and anti-β-actin. Co-labeling of N-terminal anti-Ambn antibody with anti-β-actin shows specific labeling along the distal ameloblast membrane and Tomes' Processes in *Ambn*$^{WT/WT}$ (b - d). In the case of the *Ambn*$^{\Delta L76\text{-}P86\ -/-}$ mutant, this membrane localization of N-terminal anti-Ambn antibody is lost (f - h). nuclei (blue), actin (green), Ambn (red).

Supplementary Figure 6

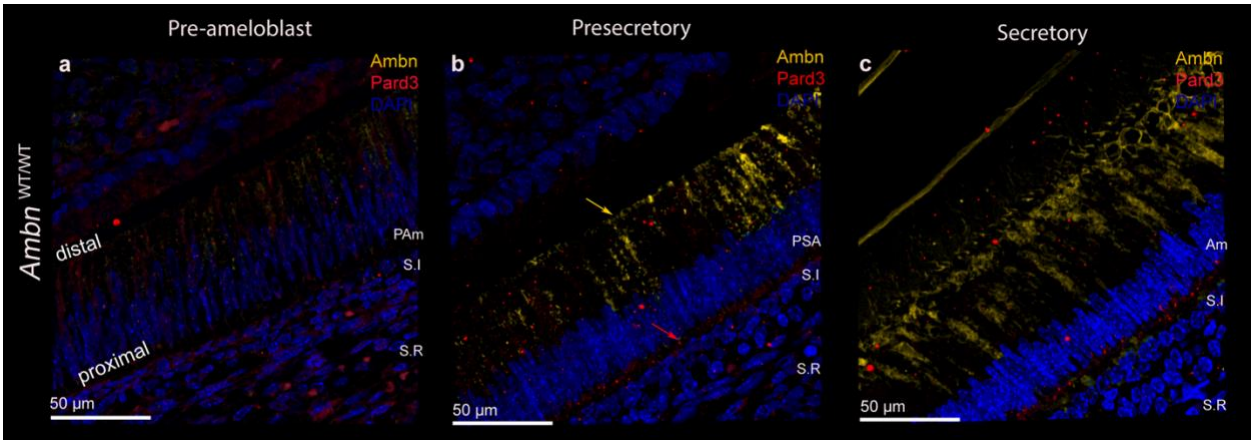

Supplementary Figure 6. (**a - c**) Stagewise immunolabeling of P8 secretory stage incisors from *Ambn*$^{WT/WT}$ mice for Pard3 (red) and full-length Ambn (yellow pseudo-color). The red arrow in b indicates the onset of a polarized Pard3 immunolocalization within the presecretory

ameloblasts. The yellow arrow in b indicates prominent Ambn immunoreactivity along the distal ameloblast cell membrane. PAm- Pre-ameloblast, PSA- presecretory ameloblast, T.P- Tomes' Processes, Am- ameloblast, S.I stratum intermedium, S.R stellate reticulum.

Supplementary Figure 7

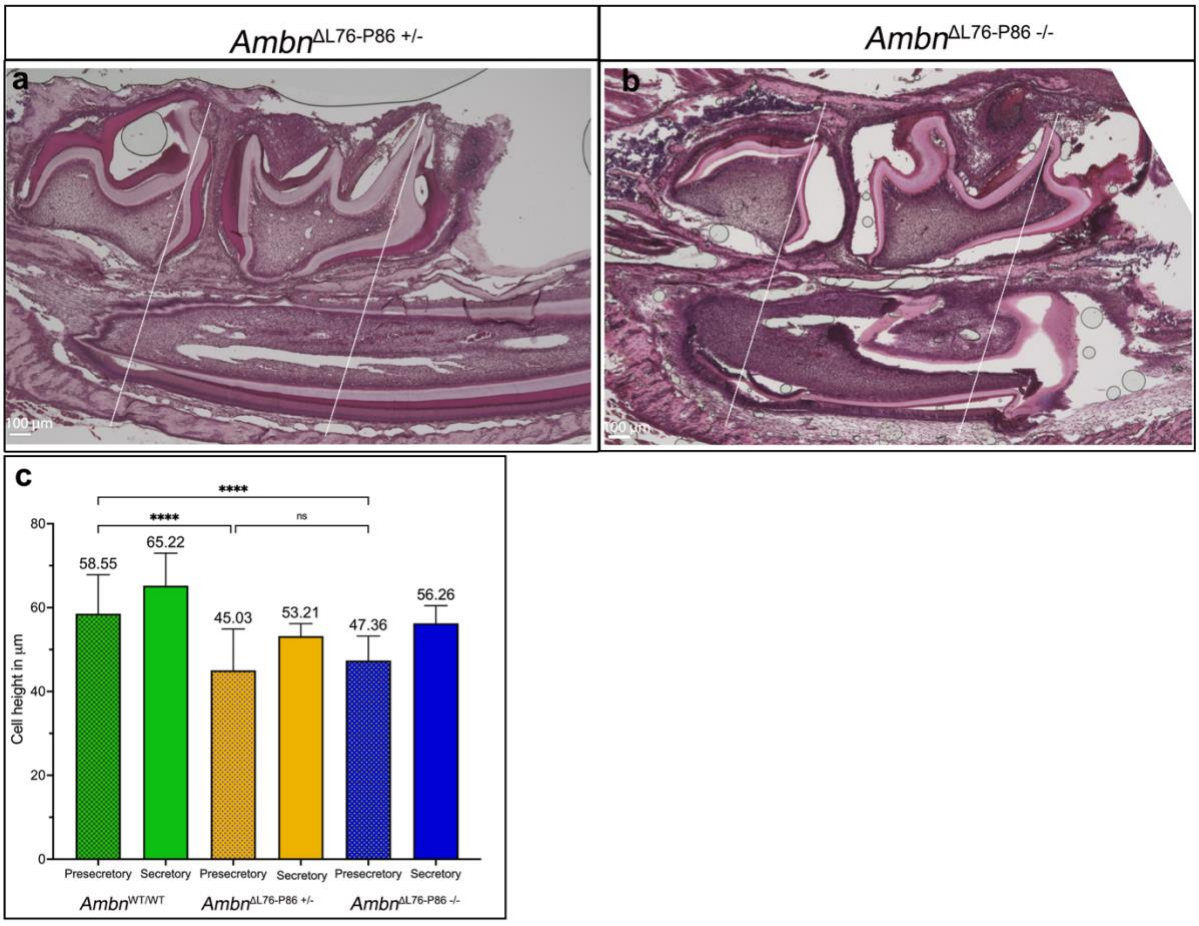

Supplementary Figure 7. (**a, b**) Anatomical landmarks used to identify secretory and presecretory stages of amelogenesis along a continuously growing incisor from P8 samples. (**c**) Height of presecretory and secretory-stage ameloblasts in *Ambn*$^{WT/WT}$ and *Ambn*$^{\Delta L76\text{-}P86}$ mutants. *Ambn*$^{WT/WT}$ (green), *Ambn*$^{\Delta L76\text{-}P86\ +/-}$ (yellow) *and Ambn*$^{\Delta L76\text{-}P86\ -/-}$ (blue). * $p < 0.05$; **$p < 0.01$, *** $p < 0.001$, n/s- not significant.

Supplementary Figure 8

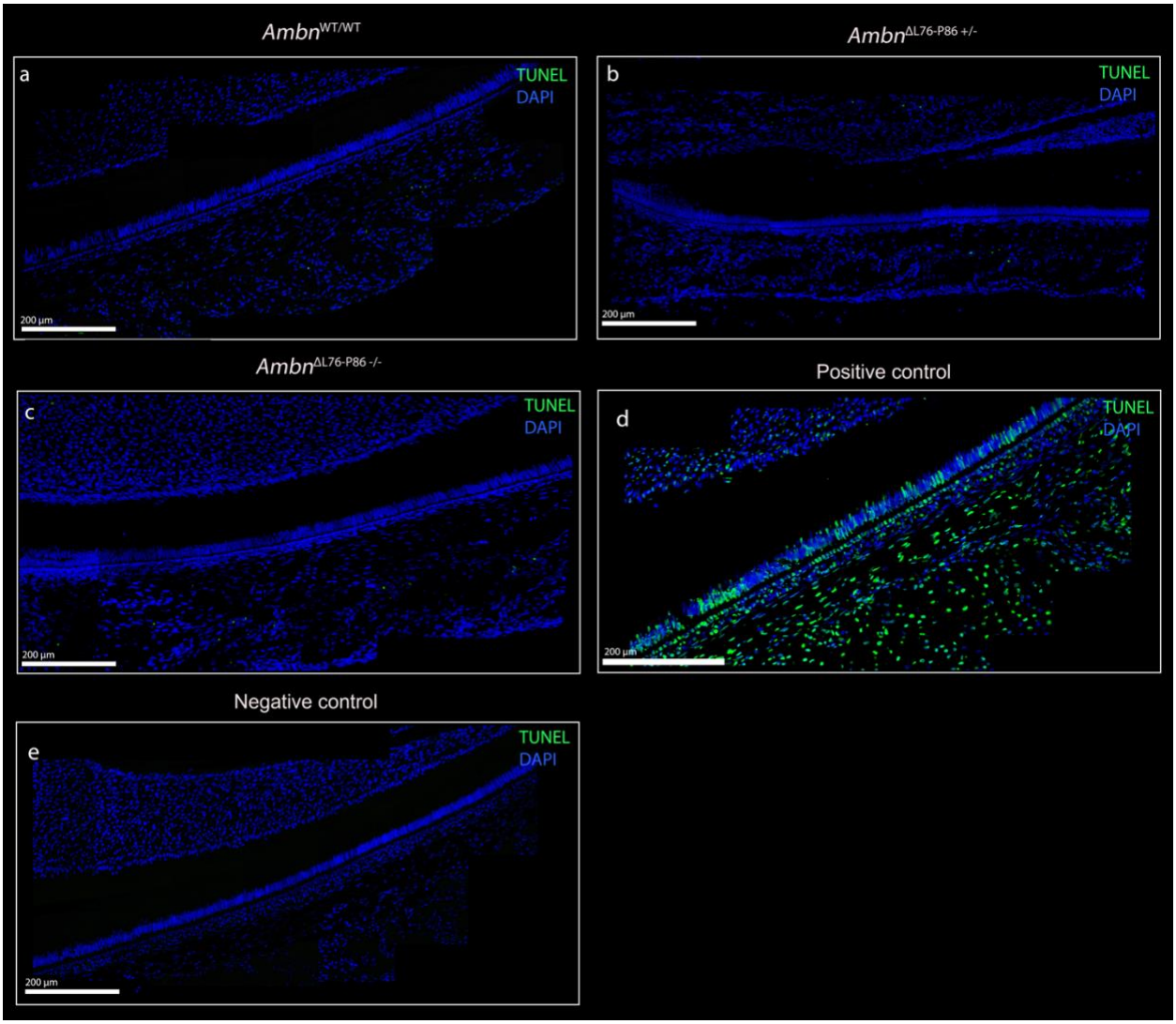

Supplementary Figure 8. (a - c). TUNEL and DAPI co-labeling of P8 mouse incisor ameloblasts from *Ambn*$^{WT/WT}$ (a), *Ambn*$^{\Delta L76\text{-}P86\ +/-}$ (b) *and Ambn*$^{\Delta L76\text{-}P86\ -/-}$ (c). **(d, e).** Positive and negative controls for TUNEL staining respectively.

Supplementary Figure 9

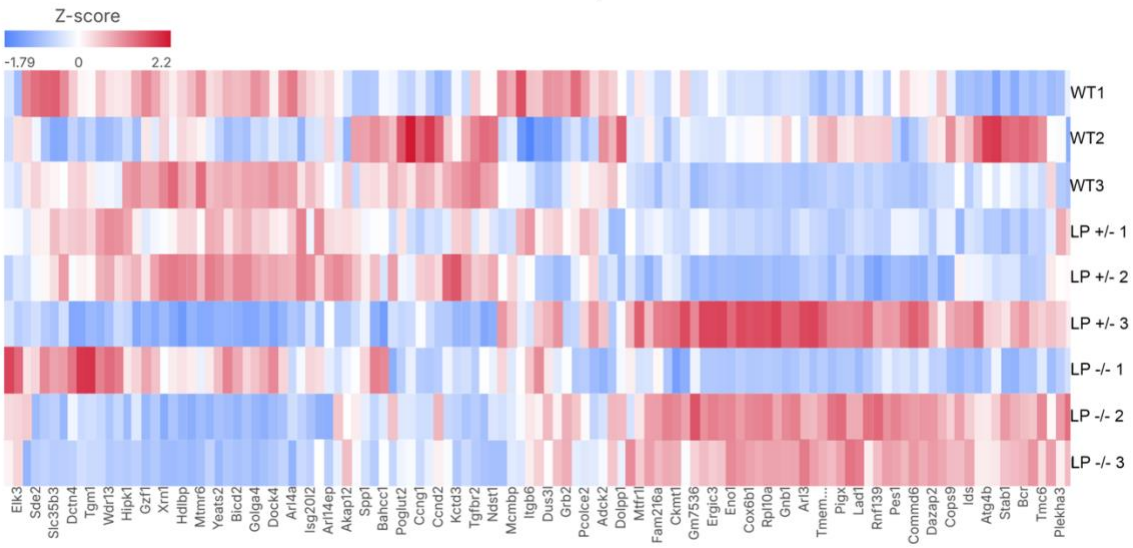

Supplementary Figure 9. Heatmap of bulk-RNA sequencing data from postnatal day 5 mandibular molars with Z-scores.

Supplementary Figure 10

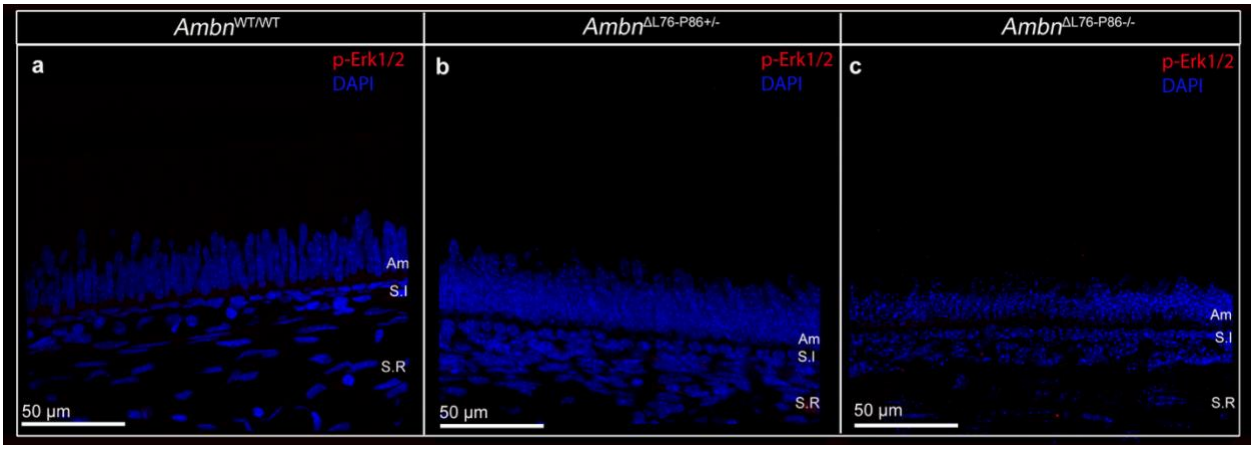

Supplementary Figure 10. (**a**) Immunolabeling for MAPK pathway mediator, p-Erk 1/2 in secretory stage ameloblasts of *Ambn*$^{WT/WT}$.(**b**) Immunolabeling for p-Erk 1/2 in in secretory stage ameloblasts of *Ambn*$^{\Delta L76\text{-}P86\ +/-}$. (**c**) Immunolabeling for p-Erk 1/2 in in secretory stage ameloblasts of *Ambn*$^{\Delta L76\text{-}P86\ -/-}$.

Supplementary Figure 11

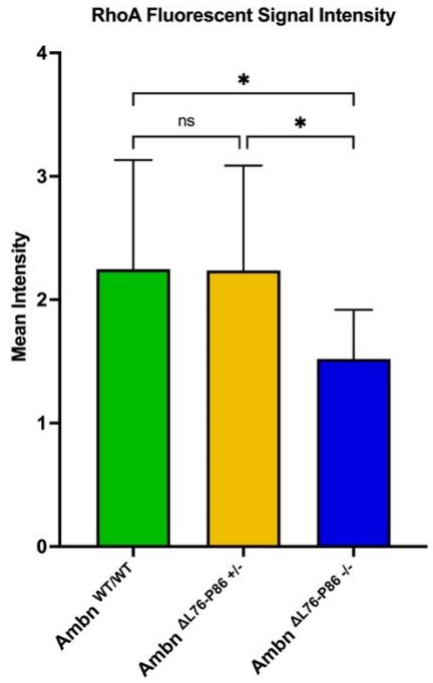

Supplementary Figure 11. Comparison of mean fluorescence intensity for P8 incisor secretory stage ameloblasts From *Ambn* $^{WT/WT}$ and *Ambn*$^{\Delta L76\text{-}P86}$ mutants stained with anti-RhoA antibody and Alexa Fluor 488 secondary. *Ambn* $^{WT/WT}$ (green), *Ambn*$^{\Delta L76\text{-}P86\ +/-}$ (yellow) and *Ambn*$^{\Delta L76\text{-}P86\ -/-}$ (blue). * $p < 0.05$.

References

1 Kegulian, N. C. & Moradian-Oldak, J. Deletion within ameloblastin multitargeting domain reduces its interaction with artificial cell membrane. *J. Struct. Biol.* **216**, 108143 (2024).

2 Su, J., Kegulian, N. C., Bapat, R. A. & Moradian-Oldak, J. Ameloblastin binds to phospholipid bilayers via a helix-forming motif within the sequence encoded by exon 5. *ACS omega* **4**, 4405-4416 (2019).

3 Su, J., Bapat, R. A. & Moradian-Oldak, J. in *Odontogenesis* 229-236 (Springer, 2019).

4 Kegulian, N. C., Langen, R. & Moradian-Oldak, J. The dynamic interactions of a multitargeting domain in ameloblastin protein with amelogenin and membrane. *Int. J. Mol. Sci.* **24**, 3484 (2023).

5 Cooley, V. *et al.* in *Developments in X-Ray Tomography XIII*. 28 (SPIE).

6 Cooley, V., Suwandi, E., Stock, S. R. & Joester, D. in *Developments in X-Ray Tomography XV*. 12-29 (SPIE).

7 Keras (2015).

8 Sullivan, C. & Kaszynski, A. PyVista: 3D plotting and mesh analysis through a streamlined interface for the Visualization Toolkit (VTK). *Journal of Open Source Software* **4**, 1450 (2019).

9 Virtanen, P. *et al.* SciPy 1.0: fundamental algorithms for scientific computing in Python. *Nature methods* **17**, 261-272 (2020).

10 Hoyer, S. & Hamman, J. xarray: ND labeled arrays and datasets in Python. (2017).

11 Harris, C. R. *et al.* Array programming with NumPy. *nature* **585**, 357-362 (2020).

12 Hunter, J. D. Matplotlib: A 2D graphics environment. *Computing in science & engineering* **9**, 90-95 (2007).

13 McKinney, W. Data structures for statistical computing in Python. *scipy* **445**, 51-56 (2010).

14 Hubbell, J. H. & Seltzer, S. M. Tables of X-ray mass attenuation coefficients and mass energy-absorption coefficients 1 keV to 20 MeV for elements Z= 1 to 92 and 48

additional substances of dosimetric interest. (National Inst. of Standards and Technology-PL, Gaithersburg, MD (United ..., 1995).

15 Humphries, M. J. Cell adhesion assays. *Extracellular Matrix Protocols: Second Edition*, 203-210 (2009).

16 Su, J., Bapat, R., Visakan, G. & Moradian-Oldak, J. An Evolutionarily Conserved Helix Mediates Ameloblastin-Cell Interaction. *J. Dent. Res.*, 0022034520918521 (2020).